Lattice-Matched Bimetallic CuPd-Graphene Nanocatalysts for Facile Conversion of Biomass-Derived Polyols to Chemicals

Xin Jin,[†] Lianna Dang,[‡] Jessica Lohrman,[‡] Bala Subramaniam,[†] Shenqiang Ren,[‡,*] and Raghunath V. Chaudhari[†,*]

[†]Center for Environmentally Beneficial Catalysis, Department of Chemical & Petroleum Engineering, University of Kansas, 1501 Wakarusa Drive, Lawrence, Kansas 66047, United States and [‡]Department of Chemistry, University of Kansas, 1251 Wescoe Hall Drive, Lawrence, Kansas 66045, United States

ABSTRACT A bimetallic nanocatalyst with unique surface configuration displays extraordinary performance for converting biomass-derived polyols to chemicals, with potentially much broader applications in the design of novel catalysts for several reactions of industrial relevance. The synthesis of nanostructured metal catalysts containing a large population of active surface facets is critical to achieve high activity and selectivity in catalytic reactions. Here, we describe a new strategy for synthesizing copper-based nanocatalysts on reduced graphene oxide support in which the catalytically active {111} facet is achieved as the dominant surface by lattice-match engineering. This method yields highly active Cu-graphene catalysts (turnover frequency = 33−114 mol/g atom Cu/h) for converting biopolyols (glycerol, xylitol, and sorbitol) to value-added chemicals, such as lactic acid and other useful co-products consisting of diols and linear alcohols. Palladium incorporation in the Cu-graphene system in trace amounts results in a tandem synergistic system in which the hydrogen generated *in situ* from polyols is used for sequential hydrogenolysis of the feedstock itself. Furthermore, the Pd addition remarkably enhances the overall stability of the nanocatalysts. The insights gained from this synthetic methodology open new vistas for exploiting graphene-based supports to develop novel and improved metal-based catalysts for a variety of heterogeneous catalytic reactions.

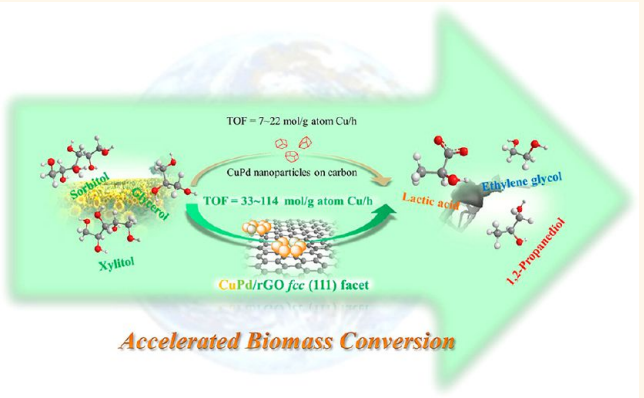

KEYWORDS: lattice · graphene · bimetallic · nanocatalysts · biomass conversion · lactic acid

One of the challenges in heterogeneous catalysis is to rationally design novel catalytic materials that perform with significantly enhanced activity, selectivity, and stability. We report here an example of rational catalyst design based on crystal lattice engineering to develop remarkably active and selective nanocatalysts for converting biomass-derived polyols to lactic acid. Replacing fossil-based feedstocks with biomass-derived ones to produce renewable fuels and chemicals is one of the major sustainability challenges facing the energy and chemical industries.[1,2] In this context, the aqueous phase hydrogenolysis (APH) of biopolyols has received much attention in recent years for producing both fuels and chemicals.[3,4] Dehydrogenation−hydrogenation (DH/H), dehydration, and aldol condensation usually involving the activation of C−O and C−H bonds of biomass molecules are regarded as the most important reactions in this technology.[5] DH/H are the key reaction steps for the synthesis of various industrial chemicals, including propanediols (PDO),[6,7] ethylene glycol (EG), and furfural alcohols,[8] as well as emerging renewables such as lactic acid (LA),[9] a new intermediate for biodegradable materials. Noble metal catalysts (*e.g.*, Pt, Ru, Rh) show high activities for DH/H reactions and hence have been studied extensively in the past decade.[6,10] However, a major issue plaguing these catalysts is the high cost and poor

* Address correspondence to shenqiang@ku.edu, rvc1948@ku.edu.

Received for review October 17, 2012 and accepted January 7, 2013.

Published online January 08, 2013
10.1021/nn304820v

selectivity. The relatively low tendency for C−O activation demands external molecular hydrogen,[6] but this unfortunately facilitates unwanted methanation and excess C−C cleavage.[11] Significant amounts of valuable hydrogen and carbon atoms are therefore lost to unwanted waste products. To overcome these limitations, much work has been reported on the design of nanocatalysts, including bimetallic formulations with controlled size, shape, and morphology.[5,6,9,10,12,13] While traditional synthesis strategies enhance the activity of the noble metal catalysts, the lack of selectivity control remains an unsolved major challenge that continues to hinder the environmental and economic viability of biomass conversion technologies.

Developing cost-effective catalytic systems such as those based on inexpensive Cu catalysts[7,14] offers a potential solution. For example, we recently discovered that Cu catalysts display robust performance for the DH/H of biopolyols, and the activation of C−O bonds does not require the addition of external hydrogen.[15] Thus the synthesis of renewable LA from glycerol is achieved at milder conditions (T = 473 K) compared with hydrothermal processes (T > 553 K).[16] This is a significant advancement over conventional technologies and opens a new area of investigation for APH technologies. However, like other traditional catalysts, Cu displays extremely low intrinsic activity (turnover frequencies, TOFs = 0.1−2.2 mol/g atom Cu/h), increased tendency for side reactions, and poor durability under harsh reactions, all of which limit its industrial applications.[15] Such catalysts might, however, be improved *via* tuning the elemental composition and altering preparation conditions.[17] Recent advances in nanoscience enable us to fabricate well-defined metal nanoparticles.[18] However, even such attempts have resulted in only marginal activity improvement (TOFs ∼ 6.8 mol/g atom Cu/h).[19]

Sizes and/or shapes of nanoparticles are not the only important factors. Even nanoparticles with different metallic facets are known to display varied catalytic activities,[18,20] thereby facilitating side reactions to form unwanted byproducts.[11,15] Recent theoretical and experimental studies suggest that some specific crystalline facets, for example, Cu{111}, might be a desired surface for performing DH/H reactions.[21−23] However, a detailed inspection of current nanometallic structures of Cu catalysts[7,17,19,24−26] reveals that the constraint of thermodynamic growth and epitaxial effect of support structures yields only a small fraction of the Cu{111} plane in those nanostructures which therefore display poor activities.[8,15,22−24] Moreover, the number of reactive surface Cu atoms also diminishes rapidly during reactions.[19,27]

Here, we report a new strategy to control the growth of Cu{111} as dominant surface facets on exotic 2-D graphene materials.[28,29] The lattice-matched Cu{111} plane has received considerable attention as the template for the 2-D growth of graphene.[30,31] Conversely, in this article, we report for the first time a novel room temperature synthesis protocol in aqueous media for selective growth of Cu nanocrystals with a dominant {111} facet by using the graphene derivative as both the growth template and catalyst support. The Cu{111} facet is energetically stable on the graphene surface due to the most proximal lattice match. In addition, we show that the 2-D Cu nanocatalysts selectively facilitate dehydrogenation and exhibit a superior enhancement in activity (TOFs = 33−114 mol/g atom Cu/h) compared to conventional nano-Cu catalysts for the conversion of polyols to LA with PDO and EG as co-products. Furthermore, we demonstrate that the integration of Pd traces with Cu-graphene catalysts results in a tandem system with excellent stability, in which hydrogen generated from LA formation can be utilized for sequential hydrogenolyis to obtain PDO, EG, and other alcoholic compounds as useful co-products. The specific application illustrated here serves only as an example and demonstrates the potential for wider application of the new synthesis methodology in heterogeneous catalysis.

RESULTS AND DISCUSSION

Synthesis of Cu-Based Nanocatalysts. The active surface facet of metal nanocrystals is a key determinant of catalyst performance. The surface facet control of mono- and bimetallic Cu-based nanocatalysts is based on crystal lattice engineering involving the Cu and the graphene support (reduced graphene oxide: rGO, Figure 1a). The Cu{111} surface plane has the closest lattice parameter match with the graphene support.[30] To minimize the lattice strain energy at the interface, the monometallic Cu or bimetallic CuPd nanoformulation tends to grow in the {111} direction onto the rGO support (Figure 1b). The aqueous phase synthesis of the Cu/rGO and CuPd/rGO nanocatalysts is based on the *in situ* reduction of Cu^{2+}, Pd^{2+}, and graphene oxide (GO) precursors at room temperature. Cu assembles into a highly ordered {111} structure which is found to be selectively formulated on the rGO surface. The {111} dominant surface plane is confirmed by using high-resolution transmission electron microscopy (HRTEM) and their fast Fourier transform (FFT) spectra, shown in Figure 1c and Figure 2a,b, respectively. The CuPd composition of the as-prepared nanocatalysts was confirmed by energy-dispersive X-ray analysis (Supporting Information Figure S2). The HRTEM images and FFT patterns exhibit the lattice spacings of Cu{111} and CuPd{111} planes and rGO support as 2.58, 2.69, and 2.70 Å respectively, exhibiting a 4.4 and 0.3% mismatch between Cu{111}/rGO and CuPd{111}/rGO surfaces, respectively. The close lattice match between CuPd{111} and rGO surfaces is responsible for the durability of the CuPd/rGO bimetallic nanocatalyst during the recycle testing, which will be elaborated in the later stability study section. Acetonitrile

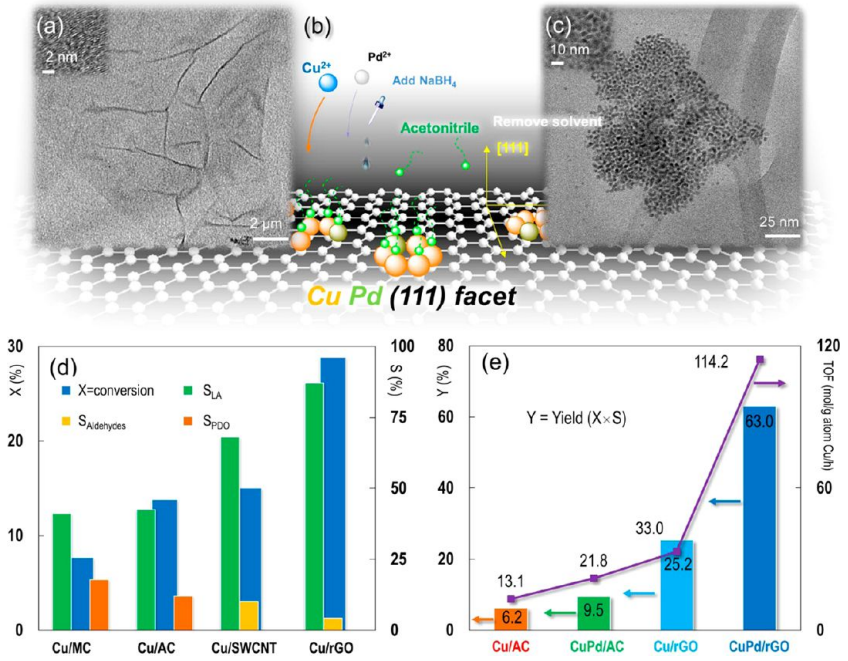

Figure 1. Synthesis of bimetallic CuPd nanopatches on graphene supports. (a) TEM image of reduced graphene oxide (rGO). The inset HRTEM image shows the rGO lattice. (b) Brief illustration of synthesis protocol: Cu^{2+} and Pd^{2+}, mixed with GO, were then reduced to the metallic state in aqueous phase with the protection of acetonitrile by hydrogen formed *in situ* by injecting $NaBH_4$, resulting in a dominant CuPd{111} surface plane. Solvent was removed before catalytic activity tests. (c) TEM image of Cu(2 wt %)−Pd(0.05 wt %) bimetallic nanocrystals on rGO support. The inset HRTEM image is of the Cu(2 wt %)−Pd(0.05 wt %)/rGO nanocatalyst. Experimental conditions in (d) and (e): glycerol, 100.0 kg/m^3; solvent, H_2O; Cu (and Pd) loading, 2 wt % (and 0.05 wt %); catalyst charge, 6.7 kg/m^3; T = 473 K; P_{N_2} = 1.4 MPa; NaOH/glycerol molar ratio, 1.1; LA, lactic acid; PDO, 1,2-propanediol; aldehydes, pyruvaldehyde and glyceraldehyde. For vertical *y*-axis, X = conversion, S = selectivity, Y = yield. Reaction time: 6 h in (d) and (e), except that TOF in (e) is calculated at $X \sim 20\%$ (reaction time = 0.5−6 h).

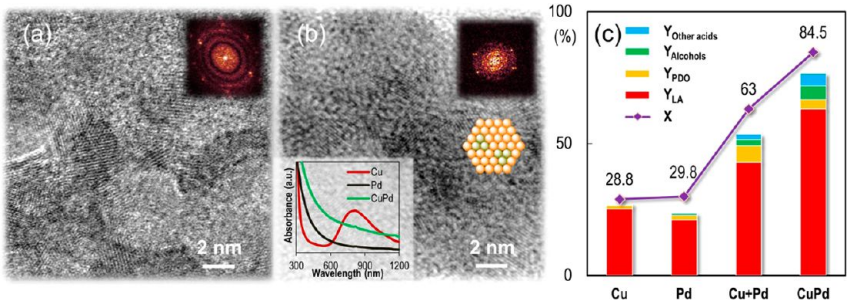

Figure 2. Structural characteristics and synergistic effect of CuPd/rGO catalyst. (a,b) HRTEM image of monometallic Cu/rGO and bimetallic CuPd/rGO hybrid nanocatalysts, respectively. The inset shows the fast Fourier transform (FFT) spectra. (b) Inset (bottom left) is the photoabsorption spectra of monometallic Cu/rGO, Pd/rGO, and bimetallic CuPd/rGO hybrid nanocatalysts. (c) Catalytic performance of Cu/rGO, Pd/rGO, the admixture Cu/rGO and Pd/rGO, and bimetallic CuPd/rGO hybrid nanocatalysts. Alcohols: methanol, ethanol, and propanols. Other acids: mainly acetic acid, traces of glycolic acid. Reaction conditions are the same as in Figure 1d.

is used to control the growth of metal nanocrystals by sharing extra electron pairs in the nitrile functional group with metal nuclei and thereby passivates the nanocrystals from oxidation during the synthesis of Cu-based catalysts.[32] For comparison, we prepared the Cu in citrate (protic solvent)−water and also in acetonitrile−water mixed solvent under purged argon gas without the rGO support, respectively. The Cu nanocrystals using the protic solvent showed immediate precipitation with a change in color to greenish blue, indicating the formation of an oxidized state (not shown here). In addition, the Cu nanocrystals using the acetonitrile route get oxidized when we remove acetonitrile after drying nanocrystals. This indicates that the protic solvent (citrate) cannot protect the oxidation by OH^- ions while the aprotic solvent (acetonitrile) is useful as a protecting solvent for the metal nanocrystals. More importantly, the rGO support sheets are critical to protect CuPd oxidation during nanocatalyst testing.[33] Cu-based catalysts supported on conventional active carbon (AC), mesoporous carbon (MC), and single-wall carbon nanotube (SWCNT) show mixed surface planes and poor activities which are comparable with published literature (details shown in the Supporting Information).[14,19,25,34]

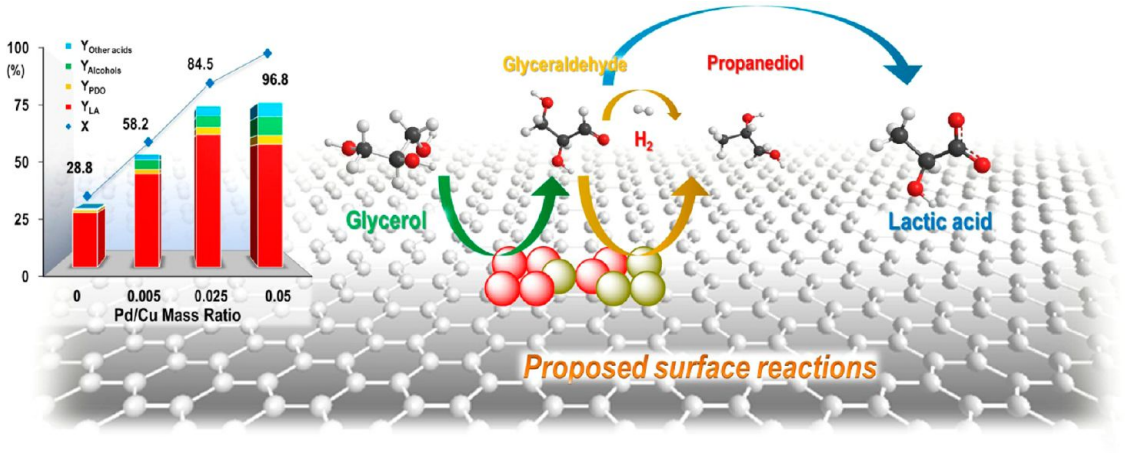

Figure 3. Conversion and product yields on Cu−Pd/rGO nanocatalysts at different Pd/Cu ratios and the proposed glycerol reaction pathways on CuPd/rGO catalysts. Reaction conditions are the same as in Figure 1d.

Structure−Performance Correlation. We performed activity tests of the nanocatalysts for the conversion of glycerol, sorbitol, and xylitol under inert atmosphere in order to evaluate their dehydrogenation and hydrodeoxygenation activities using the *in situ* formed hydrogen. In all catalyst samples, the Cu content is fixed at approximately 2 wt % and Pd content is varied. With glycerol as substrate, we find that rGO supported catalysts display superior performances compared with conventional AC, MC, and SWCNT materials (Figure 1d). For the Cu/rGO nanocatalyst, remarkable activity (TOF = 33 mol/g atom Cu/h, Figure 1e) and LA selectivity (S_{LA} = 87%, Figure 1d) are observed, while other Cu catalysts display both low activity (TOF ≈ 13 mol/g atom Cu/h, Figure 1e) and low LA selectivity (S_{LA} = 41−68%, Figure 1d). The LA yield over Cu/rGO nanocatalyst (Y_{LA} = 25%, Figure 1e) is 4 times greater than other supported Cu catalysts (Y_{LA} ∼ 6.2%). Further, the addition of Pd (0.05 wt %) to Cu/rGO nanocatalyst increases the TOF by approximately 3-fold (TOF = 114 mol/g atom Cu/h, Figure 1e) compared to the Cu/rGO catalyst. Supported CuPd on conventional carbon materials, however, only exhibits a negligible enhancement in activity and product yield. The activity of glycerol conversion and LA yield on the CuPd/rGO catalyst is approximately 5-fold greater compared to other CuPd catalysts (Figure 1e and Supporting Information). These results indicate that surface properties of carbon supports strongly affect dehydrogenation and hydro-deoxygenation activities as well as product selectivity.

To better understand the observed catalytic enhancement on the rGO support, systematic studies on catalyst nanostructure and catalytic activity were performed. The HRTEM images of Cu/rGO (Figure 2a) and CuPd/rGO hybrids (Figures 1c and 2b) reveal homogeneous distribution of the metal nanocrystals[35] with a {111} facet on rGO sheets (the average Cu and CuPd grain sizes are about 5 and 2 nm, respectively). Similarly sized Cu or CuPd nanocrystals were also synthesized on other carbon supports with randomly mixed surface planes (see Supporting Information). Considering the identical metal loadings on all catalyst samples, the distinct catalytic performances imply that the rGO support exposes the Cu atoms on the dominant reactive {111} surface plane, while a thermodynamically stable state with random growth of Cu is preferred on other carbon supports. Therefore, the surface Cu atoms on the rGO support are more efficiently utilized than conventionally prepared Cu nanoparticles, thereby decreasing catalyst costs. UV−vis absorption spectra (Figure 2b inset) show that the plasmonic resonance of Cu nanocrystals[36] disappeared after the Pd loading, which can be attributed to the formation of bimetallic CuPd ultrasmall clusters on the rGO support. Similar absorption spectra have been noted for Cu 2p and Pd 3d interaction in a Cu-rich CuPd system.[37] Unlike the formulation in colloidal phase,[38] *tiny islands* of Pd tend to be present within Cu clusters ("cluster-in-cluster" geometry, Figure 2b). The FFT pattern indicates the metal {111} growth direction and the existence of bimetallic CuPd nanoclusters by two different diffraction sets of Cu and Pd components (Figure 2b). The CuPd cluster formulation is, however, not observed with other carbon-based (AC, MC, and SWCNT) supports (details provided in Supporting Information).

A comparison study was performed to further confirm the observed synergistic coupling effect of bimetallic catalyst. Monometallic Pd/rGO catalyst (Figure 2c) displays approximately 30% conversion of glycerol but lower LA yield (Y_{LA} = 21%) compared to Cu/rGO nanocatalyst (Y_{LA} = 25%, Figure 2c). This is because Pd by itself promotes side reactions such as reforming and water gas shift (WGS).[25] Results from an admixture of Cu/rGO and Pd/rGO (Cu + Pd in Figure 2c) show that the glycerol conversion and LA yield increase to 63 and 43%, respectively, compared to individual Cu/rGO or Pd/rGO catalysts. With the (Cu + Pd) catalyst, noticeable hydrogenolysis is occurring (on the Pd metal)

by *in situ* formed hydrogen to generate increased amounts of PDO and C_{1-2} alcohols.[39] In sharp contrast, the bimetallic CuPd/rGO catalyst displays a strong synergistic effect resulting in approximately 85% glycerol conversion with a 73% total yield of products (Y_{LA} = 63%, $Y_{PDO+alcohols}$ = 10%).

Catalyst characterization results indicate that the Cu{111} surface dominates the rGO support and selectively catalyzes the dehydrogenation reaction rather than WGS[15,21] at much higher rates than other Cu surfaces. The Cu{111} surface displays higher activity and LA selectivity (S_{LA} = 74−84%) than those previously reported.[15] However, tandem hydrogenolysis is not obvious under our conditions possibly due to the low hydrogenolysis activity of Cu in an inert gas environment. The presence of Pd facilitates spillover of *in situ* formed H_2 on carbon materials;[40] the H_2 and some intermediates formed from dehydrogenation undergo tandem hydrogenolysis instead of forming waste methane and CO_2. This synergistic interaction between Cu and Pd sites and resulting tandem hydrogenolysis is clearly more remarkable on the CuPd/rGO than other catalysts, presumably due to the unique cluster-in-cluster alignment of the CuPd nanostructures.

TABLE 1. Stability Study on Cu and CuPd/rGO Catalysts[a]

			selectivity (%)			
entry	catalysts	glycerol conversion (%)	LA	PDO	alcohols	percent of metal leached
1	Cu/rGO-fresh	9.6	85.6	3.3		18.5 wt % after
2	Cu/rGO-spent	<1	41.1			1st run
3	CuPd/rGO-fresh	56.2	88.1	4.1	2.4	2.2 wt % after
4	CuPd/rGO-1st recycle	53.1	84.2	4.6	5.2	three recycles
5	CuPd/rGO-2nd recycle	52.7	85.7	3.4	3.9	
6	CuPd/rGO-3rd recycle	48.9	82.0	0.8	2.0	

[a] Glycerol, 100.0 kg/m^3; solvent, H_2O; catalysts charge = 13.2 kg/m^3; T = 413 K. Entries 1 and 2: reaction time = 6 h. Entries 3−6: reaction time = 16 h; P_{N_2} = 1.4 MPa; NaOH/glycerol molar ratio = 1.1. LA: lactic acid. PDO: 1,2-propanediol. EG: ethylene glycol. Alcohols: methanol, ethanol, and propanols. Metal content was determined by inductively coupled plasma (ICP) measurement.

Identifying an optimal Cu/Pd composition is the key to the high activity and selectivity of the proposed nanocatalysts. We therefore investigated the effect of Pd loading in nanocatalysts. The glycerol conversion is enhanced to 96% at the Pd/Cu mass ratio of 0.05, while the maximum LA yield is found to be 63% at 0.025 ratio (in Figure 3 and Table S2). With a 10% yield of PDO and linear alcohols as other co-products, the overall process shows high carbon selectivity to liquid products. At higher Pd/Cu ratios, Pd promotes side reactions, decreasing the selectivity to LA as well as other liquid products. Here, glycerol is believed to first react to form R−CH_2−O*[41,42] as a primary intermediate species which rapidly forms glyceraldehyde on surrounding Cu sites. Dehydrogenated species are instantaneously converted to LA[37,41] (with OH^-) or alcoholic chemicals[15,39] (by *in situ* formed hydrogen) in alkaline medium. This hypothesis is supported by the detection of increasing amounts of PDO and linear alcohols (including methanol, ethanol, and propanols) as the Pd/Cu ratio increases (Figure 3). Therefore, we conclude that the bimetallic CuPd clusters display a bifunctional nature for both the dehydrogenation of glycerol to form LA and *in situ* hydrogenolysis to other useful co-products without externally added hydrogen.

Stability Study. We assessed the stability of nanocatalysts (Table 1) by several catalyst recycle experiments. The results show that CuPd/rGO exhibits significant improvement in stability over the Cu/rGO catalyst. For the Cu/rGO catalyst, both inductively coupled plasma (ICP) and TEM analysis reveal that deactivation due to metal leaching (Table 1 and Figure 4a) is significant under the reaction conditions (entries 1 and 2 in Table 1). However, for the robust CuPd/rGO catalyst (Figure 4b, and entries 3−6 in Table 1), it is clear that the glycerol conversion and LA selectivity remain almost constant during recycle experiments, indicating

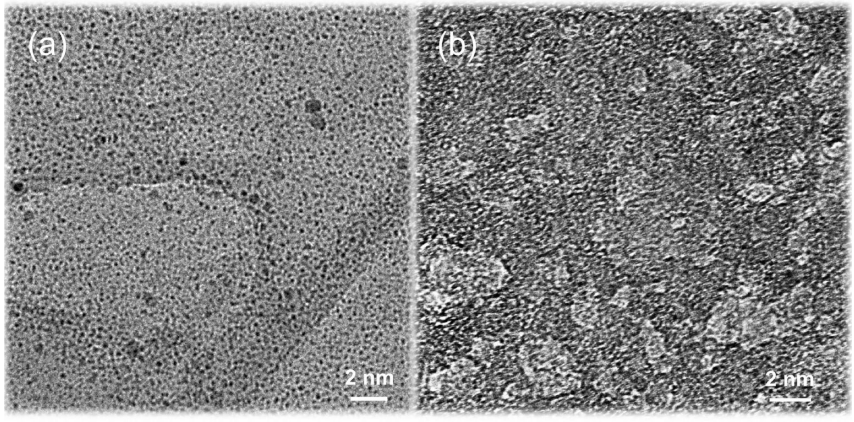

Figure 4. TEM images of (a) spent Cu/rGO (after first run) and (b) CuPd/rGO (after third recycle) catalysts. There exists obvious Cu metal leaching out on Cu/rGO during the reaction, while no significant leaching is found on the CuPd/rGO sample.

TABLE 2. Synthesis of Value-Added Chemicals from Sugar-Derived Polyol Feedstocks[a]

			selectivity (%)			
entry	substrate	conversion (%)	LA	PDO	EG	alcohols
1	xylitol	88.2	55.4	1.2	24.4	4.3
2	sorbitol	96.5	70.1	3.3	2.1	6.7

[a] Substrate, 100.0 kg/m^3; solvent, H_2O; CuPd/rGO catalyst charge = 6.7 kg/m^3; T = 473 K; reaction time = 6 h; P_{N_2} = 1.4 MPa; NaOH concentration = same as Table 1. LA: lactic acid. PDO: 1,2-propanediol. EG: ethylene glycol. Alcohols: methanol, ethanol, and propanols.

excellent stability and recyclability of the CuPd/rGO catalysts. The addition of Pd clearly increases the stability of Cu nanocatalysts. It is highly possible that the relatively stable cluster-in-cluster morphology and lattice match between metal clusters and rGO support enhances the interaction between CuPd and the graphene support. This remarkable finding will be further investigated in our laboratory to understand how nanostructure (*e.g.*, alloy, core−shell, *etc.*) and interaction between Cu and Pd affect the catalytic behavior of nanocatalysts for polyol conversion and the relevant reaction pathways.

The CuPd/rGO nanocatalysts also show remarkable performances in converting various other polyols such as xylitol (C_5) and sorbitol (C_6) to useful products. Almost complete conversions are obtained with CuPd/rGO catalyst, giving high yields of products such as LA, PDO, and ethylene glycol (see Table 2). These results show similar products as observed from the glycerol substrate. Thus, it is clear that the CuPd/rGO catalysts effectively facilitate C−C and C−O cleavage and convert bioderived polyols to LA, glycols, and linear alcohols under very mild reaction conditions. An important characteristic of Cu-based nanocatalysts is the high carbon selectivity, resulting from *in situ* H_2 generation from the substrate itself, to produce useful liquid products with significantly lower gaseous products compared to the supported noble metal catalysts.[9,43] These favorable economic and environmental attributes promote process sustainability.

CONCLUSION

In summary, a new family of surface facet-controlled bimetallic Cu-based nanocatalysts supported on the graphene derivative show exceptional activity and stability for aqueous phase biomass conversion. The novel features include the directed growth of dominant reactive surface facets of Cu nanocrystals (Cu{111}) using the graphene derivative as a 2-D template and the incorporation of Pd to achieve remarkable activity and stability enhancements. The bimetallic CuPd/rGO formulations can be potentially utilized in other applications such as DH/H of alcohols, fuel cells, catalytic CO oxidation, as well as other green energy applications. The precise nature of Pd incorporation in the CuPd/rGO formulation and the role of the graphene support deserve further investigations in order to better understand and exploit the rGO supports for the rational design and synthesis of other families of multifunctional multimetallic nanocatalysts with enhanced activity, selectivity, and stability.

MATERIALS AND METHODS

Materials. Chemicals including glycerol (>99.5%), D-sorbitol (99+%), xylitol (99+%), 1,2-propanediol (99.5+%), ethylene glycol (99.8+%), ethanol (99.5%), methanol (99.8%), and NaOH were purchased from Sigma-Aldrich. Lactic acid was purchased from Fluka and glycolic acid from Acros. Unsupported Cu_2O, $CuCl_2$, $Pd(acac)_2$, acetonitrile, and sodium borohydride ($NaBH_4$) were purchased from Sigma-Aldrich and used as received without further purification. The water used was purified through a Millipore system. Hydrogen (>99.5%) and nitrogen (>99%) were procured from Air Gas Inc. and Linweld, respectively.

Synthesis of Cu-Based rGO Catalysts. Graphene oxide was prepared in-house by a modified Hummers method starting from graphite powder (Bay Carbon, SP−1). The as-synthesized GO was dispersed in water and sonicated for 20 min. GO sheets, containing −COOH and −CHO functional groups, act as anchoring sites for the metal precursors. Treatment of precursor−GO hybrids with sodium borohydride ($NaBH_4$) resulted in precipitation of CuPd/rGO hybrids (Figure 1c). Cu/Pd weight ratio can be varied by controlling the amount of metal precursors. The resulting catalysts display superior performance compared to other carbon-supported catalysts (see Figure 1d and Table S1). Cu-based graphene nanoparticles were synthesized using $CuCl_2$ and $NaBH_4$ in a molar ratio of 6:1. $CuCl_2$ was dissolved in the GO aqueous suspension and CH_3CN (CH_3CN = 2:1 volume). $Pd(acac)_2$ was mixed at the desired mass ratio relative to Cu. Under vigorous stirring, sodium borohydride ($NaBH_4$) solution was injected drop-by-drop into the reaction medium under argon *via* a syringe pump at room temperature. The injection of the borohydride solution was continued (5−10 mL) until wine-reddish color was observed. The *in situ* reduction of Cu^{2+} and Pd^{2+} to Cu^0 and Pd^0 at room temperature is achieved with the hydrogen slowly released from $NaBH_4$. Besides, the Cu−Pd bimetallic structure is mostly a monolayer on rGO, which is well-controlled by the existence of acetonitrile. Acetonitrile is eventually removed by solid−liquid separation (*e.g.*, centrifuge) and drying the catalyst in a vacuum oven at 80 °C overnight. The C/O ratio of rGO employed was determined to be in the range of ∼10−20 atom % by Fourier transform infrared (FT−IR) and NMR spectroscopies.

Activity Tests. Catalytic tests were carried out in a high-temperature, high-pressure, magnetically stirred multiple batch slurry reactor setup. PTFE liners were used in each test in order to avoid the catalytic effect of reactor materials at elevated temperature (413−473 K) in the presence of alkali. For a typical test, a certain amount of polyols and sodium hydroxide was dissolved in 15 mL of water. The solvent in the nanocatalyst slurry was first removed, and then the solid catalysts were sealed in 15 mL of water before activity tests. Then, the substrate and alkali solution were added slowly into the catalyst slurry and mixed completely before injecting into the Parr reactor. The reactor was then sealed and purged three times with N_2. The reactor was first heated to a desired temperature followed by introduction of N_2 up to 1.4 MPa pressure. The reaction was started by increasing the agitation speed to 500 rpm. After a batch reaction, the contents in the reactor were cooled to room

temperature, and the gas phase products were analyzed using GC. GC results show that almost no gases (other than N_2) are detected in the gas phase following reaction (gas products selectivity <0.1%). Then, the reactor was opened and the pH value of liquid samples was measured (pH >11). Then, 20 mL of sulfuric acid solution in water was added to neutralize the liquid products. The pH value was measured again (pH <5), and a final volume of the liquid sample was also noted before analysis using HPLC [a Rezex ROA-organic acid H^+ (8%) column, 0.005 N aqueous H_2SO_4 as a mobile phase and a RI detector]. The analytical results from the HPLC were combined to get a quantitative assessment of each component and calculation of conversion/selectivity profiles.

The typical carbon balance for Cu/rGO and CuPd/rGO catalysts ranges from approximately 85 to 97%. When Pd content is higher (*i.e.*, Pd/Cu mass ratio >0.05 w/w), a lower carbon balance (65−78%) is estimated due to the loss of carbon as CO_2 (*via* WGS) that is captured by hydroxide ions as carbonate but not analyzed and accounted for.

Similar procedures were followed for the catalyst recycle studies. After each run, the liquid products and solid catalysts were separated and new feedstock was charged immediately into the reactor with the used catalysts.

Conflict of Interest: The authors declare no competing financial interest.

Acknowledgment. X.J. acknowledges the scholarship from China Scholarship Council. S.R. acknowledges support from the University of Kansas Start-Up fund, New Faculty General Research Fund, and DOE (DESC0005448). Partial support from the United States Department of Agriculture (USDA/NIFA Award 2011-10006-30362) is gratefully acknowledged.

Supporting Information Available: Additional experimental details, figures, and tables. This material is available free of charge *via* the Internet at http://pubs.acs.org.

REFERENCES AND NOTES

1. Cortright, R. D.; Davda, R. R.; Dumesic, J. A. Hydrogen from Catalytic Reforming of Biomass-Derived Hydrocarbons in Liquid Water. *Nature* **2002**, *418*, 964–967.
2. Huber, G. W.; Iborra, S.; Corma, A. Synthesis of Transportation Fuels from Biomass: Chemistry, Catalysts, and Engineering. *Chem. Rev.* **2006**, *106*, 4044–4098.
3. Huber, G. W.; Cortright, R. D.; Dumesic, J. A. Renewable Alkanes by Aqueous-Phase Reforming of Biomass-Derived Oxygenates. *Angew. Chem., Int. Ed.* **2004**, *43*, 1549–1551.
4. Huber, G. W.; Chheda, J. N.; Barrett, C. J.; Dumesic, J. A. Production of Liquid Alkanes by Aqueous-Phase Processing of Biomass-Derived Carbohydrates. *Science* **2005**, *308*, 1446–1450.
5. Kunkes, E. L.; Simonetti, D. A.; West, R. M.; Serrano-Ruiz, J. C.; Gartner, C. A.; Dumesic, J. A. Catalytic Conversion of Biomass to Monofunctional Hydrocarbons and Targeted Liquid-Fuel Classes. *Science* **2008**, *322*, 417–421.
6. Ma, L.; He, D. H. Hydrogenolysis of Glycerol to Propanediols over Highly Active Ru−Re Bimetallic Catalysts. *Top. Catal.* **2009**, *52*, 834–844.
7. Yuan, Z. L.; Wang, L. N.; Wang, J. H.; Xia, S. X.; Chen, P.; Hou, Z. Y.; Zheng, X. M. Hydrogenolysis of Glycerol over Homogenously Dispersed Copper on Solid Base Catalysts. *Appl. Catal., B* **2011**, *101*, 431–440.
8. Li, N.; Tompsett, G. A.; Huber, G. W. Renewable High-Octane Gasoline by Aqueous-Phase Hydrodeoxygenation of C-5 and C-6 Carbohydrates over Pt/Zirconium Phosphate Catalysts. *ChemSusChem* **2010**, *3*, 1154–1157.
9. Maris, E. P.; Davis, R. J. Hydrogenolysis of Glycerol over Carbon-Supported Ru and Pt Catalysts. *J. Catal.* **2007**, *249*, 328–337.
10. King, D. L.; Zhang, L. A.; Xia, G.; Karim, A. M.; Heldebrant, D. J.; Wang, X. Q.; Peterson, T.; Wang, Y. Aqueous Phase Reforming of Glycerol for Hydrogen Production over Pt−Re Supported on Carbon. *Appl. Catal., B* **2010**, *99*, 206–213.
11. Torres, A.; Roy, D.; Subramaniam, B.; Chaudhari, R. V. Kinetic Modeling of Aqueous-Phase Glycerol Hydrogenolysis in a Batch Slurry Reactor. *Ind. Eng. Chem. Res.* **2010**, *49*, 10826–10835.
12. Maris, E. P.; Ketchie, W. C.; Murayama, M.; Davis, R. J. Glycerol Hydrogenolysis on Carbon-Supported PtRu and AuRu Bimetallic Catalysts. *J. Catal.* **2007**, *251*, 281–294.
13. Chia, M.; Pagan-Torres, Y. J.; Hibbitts, D.; Tan, Q. H.; Pham, H. N.; Datye, A. K.; Neurock, M.; Davis, R. J.; Dumesic, J. A. Selective Hydrogenolysis of Polyols and Cyclic Ethers over Bifunctional Surface Sites on Rhodium−Rhenium Catalysts. *J. Am. Chem. Soc.* **2011**, *133*, 12675–12689.
14. Yuan, Z. L.; Wang, J. H.; Wang, L. N.; Xie, W. H.; Chen, P.; Hou, Z. Y.; Zheng, X. M. Biodiesel Derived Glycerol Hydrogenolysis to 1,2-Propanediol on Cu/MgO Catalysts. *Bioresour. Technol.* **2010**, *101*, 7088–7092.
15. Roy, D.; Subramaniam, B.; Chaudhari, R. V. Cu-Based Catalysts Show Low Temperature Activity for Glycerol Conversion to Lactic Acid. *ACS Catal.* **2011**, *1*, 548–551.
16. Shen, Z.; Jin, F. M.; Zhang, Y. L.; Wu, B.; Kishita, A.; Tohji, K.; Kishida, H. Effect of Alkaline Catalysts on Hydrothermal Conversion of Glycerin into Lactic Acid. *Ind. Eng. Chem. Res.* **2009**, *48*, 8920–8925.
17. Huang, Z. W.; Cui, F.; Kang, H. X.; Chen, J.; Zhang, X. Z.; Xia, C. G. Highly Dispersed Silica-Supported Copper Nanoparticles Prepared by Precipitation-Gel Method: A Simple but Efficient and Stable Catalyst for Glycerol Hydrogenolysis. *Chem. Mater.* **2008**, *20*, 5090–5099.
18. Somorjai, G. A.; Frei, H.; Park, J. Y. Advancing the Frontiers in Nanocatalysis, Biointerfaces, and Renewable Energy Conversion by Innovations of Surface Techniques. *J. Am. Chem. Soc.* **2009**, *131*, 16589–16605.
19. Bienholz, A.; Schwab, F.; Claus, P. Hydrogenolysis of Glycerol over a Highly Active CuO/ZnO Catalyst Prepared by An Oxalate Gel Method: Influence of Solvent and Reaction Temperature on Catalyst Deactivation. *Green Chem.* **2010**, *12*, 290–295.
20. Lee, I.; Morales, R.; Albiter, M. A.; Zaera, F. Synthesis of Heterogeneous Catalysts with Well Shaped Platinum Particles To Control Reaction Selectivity. *Proc. Natl. Acad. Sci. U.S.A.* **2008**, *105*, 15241–15246.
21. Gokhale, A. A.; Dumesic, J. A.; Mavrikakis, M. On the Mechanism of Low-Temperature Water Gas Shift Reaction on Copper. *J. Am. Chem. Soc.* **2008**, *130*, 1402–1414.
22. Madon, R. J.; Braden, D.; Kandoi, S.; Nagel, P.; Mavrikakis, M.; Dumesic, J. A. Microkinetic Analysis and Mechanism of the Water Gas Shift Reaction over Copper Catalysts. *J. Catal.* **2011**, *281*, 1–11.
23. Greeley, J.; Mavrikakis, M. Methanol Decomposition on Cu(111): A DFT Study. *J. Catal.* **2002**, *208*, 291–300.
24. Balaraju, M.; Rekha, V.; Prasad, P. S. S.; Prasad, R. B. N.; Lingaiah, N. Selective Hydrogenolysis of Glycerol to 1,2 Propanediol over Cu−ZnO Catalysts. *Catal. Lett.* **2008**, *126*, 119–124.
25. Xia, S. X.; Yuan, Z. L.; Wang, L. N.; Chen, P.; Hou, Z. Y. Hydrogenolysis of Glycerol on Bimetallic Pd-Cu/Solid-Base Catalysts Prepared *via* Layered Double Hydroxides Precursors. *Appl. Catal., A* **2011**, *403*, 173–182.
26. Blanc, B.; Bourrel, A.; Gallezot, P.; Haas, T.; Taylor, P. Starch-Derived Polyols for Polymer Technologies: Preparation by Hydrogenolysis on Metal Catalysts. *Green Chem.* **2000**, *2*, 89–91.
27. Kameoka, S.; Tanabe, T.; Tsai, A. P. Spinel $CuFe_2O_4$: A Precursor for Copper Catalyst with High Thermal Stability and Activity. *Catal. Lett.* **2005**, *100*, 89–93.
28. Meyer, J. C.; Geim, A. K.; Katsnelson, M. I.; Novoselov, K. S.; Booth, T. J.; Roth, S. The Structure of Suspended Graphene Sheets. *Nature* **2007**, *446*, 60–63.
29. Geim, A. K. Graphene: Status and Prospects. *Science* **2009**, *324*, 1530–1534.
30. Li, X. S.; Cai, W. W.; An, J. H.; Kim, S.; Nah, J.; Yang, D. X.; Piner, R.; Velamakanni, A.; Jung, I.; Tutuc, E.; *et al.* Large-Area Synthesis of High-Quality and Uniform Graphene Films on Copper Foils. *Science* **2009**, *324*, 1312–1314.
31. Wang, Y.; Zheng, Y.; Xu, X. F.; Dubuisson, E.; Bao, Q. L.; Lu, J.; Loh, K. P. Electrochemical Delamination of CVD-Grown

Graphene Film: Toward the Recyclable Use of Copper Catalyst. *ACS Nano* **2011**, *5*, 9927–9933.
32. Huang, J. H.; Chen, H. J.; Hsieh, C. C.; Lee, G. H.; Peng, S. M. Synthesis and Characterization Five-Coordinate Molybdenum Compounds Bearing Bi- or Tridentate Substituted Pyrrole Ligands: Molecular Structures of $\{Mo(NC_6H_3Pr^i_2\text{-}2,6)_2R[NC_4H_3(CH_2NMe_2)\text{-}2]\}$ and $\{Mo(NC_6H_3Pr^i_2\text{-}2,6)_2Cl[NC_4H_2(CH_2NMe_2)_2\text{-}2,5]\}$, Where R = Cl, Me, Bu. *Inorg. Chim. Acta* **2011**, *321*, 142–148.
33. Chen, S. S.; Brown, L.; Levendorf, M.; Cai, W. W.; Ju, S. Y.; Edgeworth, J.; Li, X. S.; Magnuson, C. W.; Velamakanni, A.; Piner, R. D.; *et al.* Oxidation Resistance of Graphene-Coated Cu and Cu/Ni Alloy. *ACS Nano* **2011**, *5*, 1321–1327.
34. Rioux, R. M.; Vannice, M. A. Hydrogenation/Dehydrogenation Reactions: Isopropanol Dehydrogenation over Copper Catalysts. *J. Catal.* **2003**, *216*, 362–376.
35. Balogh, L.; Tomalia, D. A. Poly(amidoamine) Dendrimer-Templated Nanocomposites. 1. Synthesis of Zerovalent Copper Nanoclusters. *J. Am. Chem. Soc.* **1998**, *120*, 7355–7356.
36. Chan, G. H.; Zhao, J.; Hicks, E. M.; Schatz, G. C.; Van Duyne, R. P. Plasmonic Properties of Copper Nanoparticles Fabricated by Nanosphere Lithography. *Nano Lett.* **2007**, *7*, 1947–1952.
37. Rao, R. S.; Bansil, A.; Asonen, H.; Pessa, M. Electronic-Structure of Copper-Rich Copper−Palladium Alloys. *Phys. Rev. B* **1984**, *29*, 1713–1721.
38. Toshima, N.; Wang, Y. Preparation and Catalysis of Novel Colloidal Dispersions of Copper Noble-Metal Bimetallic Clusters. *Langmuir* **1994**, *10*, 4574–4580.
39. Roy, D.; Subramaniam, B.; Chaudhari, R. V. Aqueous Phase Hydrogenolysis of Glycerol to 1,2-Propanediol without External Hydrogen Addition. *Catal. Today* **2010**, *156*, 31–37.
40. Contescu, C. I.; Brown, C. M.; Liu, Y.; Bhat, V. V.; Gallego, N. C. Detection of Hydrogen Spillover in Palladium-Modified Activated Carbon Fibers during Hydrogen Adsorption. *J. Phys. Chem. C* **2009**, *113*, 5886–5890.
41. Davda, R. R.; Shabaker, J. W.; Huber, G. W.; Cortright, R. D.; Dumesic, J. A. A Review of Catalytic Issues and Process Conditions for Renewable Hydrogen and Alkanes by Aqueous-Phase Reforming of Oxygenated Hydrocarbons over Supported Metal Catalysts. *Appl. Catal., B* **2005**, *56*, 171–186.
42. Zope, B. N.; Hibbitts, D. D.; Neurock, M.; Davis, R. J. Reactivity of the Gold/Water Interface during Selective Oxidation Catalysis. *Science* **2010**, *330*, 74–78.
43. Auneau, F.; Michel, C.; Delbecq, F.; Pinel, C.; Sautet, P. Unravelling the Mechanism of Glycerol Hydrogenolysis over Rhodium Catalyst through Combined Experimental−Theoretical Investigations. *Chem.—Eur. J.* **2011**, *17*, 14288–14299.